Some Characteristics of Stirred Vessel Flows of Dilute Polymer Solutions Powered by a Hyperboloid Impeller

A. S. Cavadas and F. T. Pinho

Centro de Estudos de Fenómenos de Transporte, Departamento de Engenharia Mecânica, Escola de Engenharia, Campus de Azurém, 4800–058 Guimarães, Portugal

Measurements of the power consumption and mean and turbulent velocities in the wall jet of a stirred vessel flow, powered by a hyperboloid impeller, were carried out. The fluids were aqueous solutions of tylose, CMC and xanthan gum (XG), at weight concentrations ranging from 0.1% to 0.6%, which exhibited varying degrees of shear-thinning and viscoelasticity. The hyperboloid impeller parameter k of Metzner and Otto (1957) was found to be equal to 27.2 ±4. In the Reynolds number range of 10^3 to 3×10^4 the mixing power was reduced for all non-Newtonian fluids, but never by more than 13%. The flows of the 0.2% CMC and 0.2% XG solutions were found to be less turbulent than those of water, especially for the latter fluid where a reduction in axial rms in excess of 50% was found in the wall jet. This was attributed to elasticity effects and especially to the high zero shear viscosity of the latter fluid.

On a effectué des mesures de la consommation d'énergie et des vitesses moyennes et turbulentes dans le jet à la paroi pour un écoulement en réservoir agité muni d'une turbine hyperboloïde. Les fluides étudiés sont des solutions aqueuses de tylose, de CMC et de gomme de xanthane (XG), à des concentrations massiques comprises entre 0,1 % et 0,6 %, qui montrent différents niveaux de rhéofluidisance et de viscoélasticité. On a trouvé que le paramètre de turbine hyperboloïde k de Metzner et Otto (1957) était égal à 27,2 ± 4. Dans la gamme du nombre de Reynolds de 10^3 à 3×10^4, la puissance de mélange a été réduite pour tous les fluides non newtoniens, mais jamais de plus de 13 %. Les écoulements des solutions de 0,2 % de CMC et de 0,2 % de XG s'avèrent moins turbulents que ceux de l'eau, en particulier pour le dernier fluide où on constate une réduction du rms axial supplémentaire de 50 % dans le jet à la paroi. Cela est attribué aux effets de l'élasticité et en particulier à la forte viscosité à faible cisaillement du dernier fluide.

Keywords: stirred vessels, hyperboloid impeller, polymer solutions, mixing.

Stirred vessels are required by many industries both in processing as well as in environmental applications, such as in waste water treatment plants. They fulfil a large variety of tasks from the mixing of liquids and suspensions to blending, without and with aeration for oxidation or nitrification, and often include heat transfer and chemical reactions. The large variety of applications, fluids and objectives require different vessel shapes and types of agitator from the bulky low rotational speed impellers, required for very viscous fluids, to small high-speed rotating devices for low viscosity fluids.

The use of hyperboloid impellers is advantageous in processes involving low viscosity fluids and microorganisms, one such case being waste water treatment plants (see Invent GmbH Web site). This advantage stems from the capacity of the hyperboloid impeller to sustain an overall gentle flow that avoids destruction of useful microorganisms (Höfken et al. 1991, 1994) at the same time that it provides a reasonable degree of mixing at a fairly low power. Given its application in waste water treatment plants, which deal with non-Newtonian fluids (Monteiro and Valente, 1996), it is necessary to extend previous investigations with Newtonian fluids by Höfken et al. (1991, 1994), Pinho et al. (1997, 2000), Nouri and Whitelaw (1994) and Ismailov et al. (1997) to low viscosity non-Newtonian fluids, and later to solid-liquid and solid-liquid-gas fluid flows.

The objective of this paper is to characterize the power consumption and the corresponding circulating flow rate, and hence to define a hydrodynamic efficiency, in stirred vessel flows powered by an hyperboloid impeller when operating with various types of shear-thinning, viscoelastic, dilute and semi-dilute polymer solutions. The measurements will also allow a qualitative picture of the turbulent flow field to identify areas of future research with these non-Newtonian fluids.

The quantities and problems underlying the various measurements are presented in the next section and are followed by a description of the experimental facility and instrumentation. Prior to the discussion of the results, the rheological characteristics of the fluids are presented. A summary of the main conclusions ends the paper.

Preliminaries

For Newtonian fluids the power consumption in a stirred vessel depends on fluid properties, geometrical parameters and flow quantities and the

* *Author to whom correspondence may be addressed. E-mail address: fpinho@dem.uminho.pt.*

functional relationship amongst these quantities can be normalized for single-phase fluids as,

$$Ne \equiv \frac{P}{\rho N^3 D^5} = f\left(Re \equiv \frac{\rho N D^2}{\eta_c}, Fr \equiv \frac{N^2 D}{g}, \frac{D}{T}, \frac{C}{T}, \frac{H}{T}, \text{impeller} \right) \quad (1)$$

where other geometric nondimensional numbers have been omitted. In Equation (1) *Ne* is the Newton number (alternatively called power number) and the first and second numbers on the right-hand side are the Reynolds number and the Froude number, respectively. Regarding the dimensional quantities, *P* is the mixing power, *N* is the rotational speed traditionally in [rps], *g* is the acceleration of gravity and the geometrical parameters *D, H, C* and *T* are explained in Figure 1. Except for *N*, all other quantities are in SI units. Here, Froude number effects are negligible because the baffles, and the low flow velocities near the fluid surface, keep the free-surface flat.

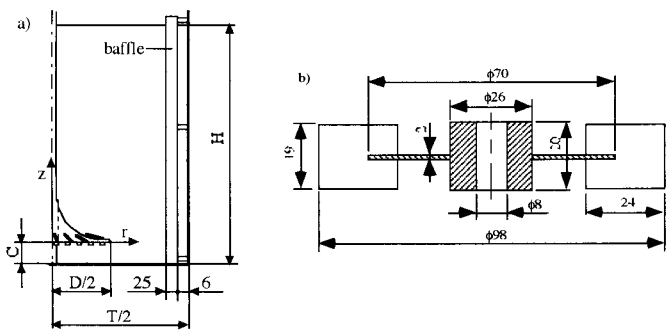

Figure 1. Geometric representation of the stirred vessel and the Rushton impeller: (a) the stirred vessel; (b) Rushton impeller.

Non-Newtonian fluids modify Equation (1) in two ways. For purely viscous fluids of variable viscosity the issue of the adequate characteristic viscosity η_c for the calculation of the Reynolds number arises. If the fluid is elastic the corresponding fluid properties gives rise to a new nondimensional number, such as the Deborah number *De* defined as

$$De = \lambda N \quad (2)$$

where λ is a relaxation time that can be related to the ratio between the first normal stress coefficient and the fluid viscosity.

The determination of the characteristic viscosity for stirred vessel flows was addressed a long time ago by Metzner and Otto (1957) and Calderbank and Moo-Young (1959), who devised a strategy aimed at comparing *Ne-Re* data obtained under different geometrical conditions and with different impellers. They were inspired by the definition of an apparent viscosity in laminar pipe flow.

The characteristic viscosity η_c, which they called apparent viscosity, was defined in such a way that the *Ne-Re* relationship for non-Newtonian fluids coincides with the *Ne-Re* relationship for Newtonian fluids in the laminar flow regime, at identical rotational speeds and other flow conditions being equal. Metzner and Otto (1957) proceeded to relate the apparent viscosity with a characteristic shear rate γ_c via the fluid rheogram or viscosity equation and for that purpose assumed that the flow in the impeller region was characterized by an average shear rate that was linearly related to the rotational speed, Equation (3)

$$\dot{\gamma}_c = kN \quad (3)$$

This is a convenient and simple procedure for engineering purposes and has since been adopted in the specialized literature. Equation (3) is valid under conditions of negligible inertia and fluid elasticity as has been shown by numerous works in the literature. The main problem is that often the fluids required to determine Metzner and Otto's coefficient *k* need to be very concentrated and thus are highly elastic compared to the dilute solutions for which the value of *k* is to be used under relevant mixing flow situations. This creates difficulties because the shear-thinning intensity and viscoelasticity of the fluids increase dramatically with polymer concentration and in the literature (Ulbrecht and Carreau, 1985) there are many reports of both an increase and a decrease in power consumption due to fluid elasticity in the laminar flow regime.

The effects of fluid shear-thinning and elasticity on Metzner and Otto's coefficient have been investigated experimentally by Zhou et al. (2000) and Carreau et al. (1993) for a double planetary mixer and a helical ribbon, respectively. The former found *k* to decrease as fluids became more shear-thinning but its impact on deviations of the inverse linearity of the *Ne-Re* plot at low Reynolds numbers was unnoticed. Furthermore, no effect due to fluid elasticity was seen at very low Reynolds numbers, confirming similar findings by Carreau et al. (1993) for the helical ribbon. However, at higher Reynolds numbers within the laminar regime Carreau et al. (1993) found elasticity to increase the power consumption. The recent numerical investigations of Bertrand et al. (1999) for the helical ribbon confirmed the findings of Carreau et al. (1993): increased power consumption due to fluid elasticity only takes place above critical Reynolds numbers, possibly due to normal stress effects since no differences in flow pattern were observed. At lower Reynolds numbers, where Metzner and Otto's procedure should be applied, no effects of fluid elasticity were seen. These are not totally unsurprising conclusions because earlier works used many fluids having different degrees of shear-thinning and elasticity and yet found values of *k* in reasonable agreement.

Other elasticity effects have been noticed in stirred vessels at low Reynolds numbers: for large polymer concentrations of CMC and xanthan gum (up to 1.4% and 4.5%, respectively) Solomon et al. (1981) have observed a reversal of the secondary flow pattern in the vicinity of a Rushton impeller and related this change to fluid viscoelasticity measured by the first normal stress difference. Secondary flow reversals also occur on simpler geometries such as in the viscoelastic flow in the vicinity of a rotating sphere (Boger and Walters, 1993).

With the very viscous fluids required by Metzner and Otto's method the flow becomes localized in the vicinity of the impeller forming caverns of motion. This is bound to occur with impellers designed for large Reynolds number flows

working with highly viscous non-Newtonian fluids (Solomon et al. 1981) such as turbine agitators or Rushton impellers, and was observed with the hyperboloid mixer. Hence, under these flow conditions the flow differs significantly from the normal flow for which the impeller was designed.

Parameter k is unknown for the hyperboloid agitator and its determination for the configuration described in the next section, the most widely used in industry (Höfken et al. 1994), is one of the objectives of the present work. However, a more extensive set of non-Newtonian fluids than the one used here is required to arrive at a more definite value.

A low power number impeller is not necessarily more efficient. The power consumption should be confronted with output quantities and, from an hydrodynamic point of view, a useful concept is that of circulation flow rate Q_c, which is the maximum flow rate in circulation from the bottom to the top of the vessel. An alternative would be the pumping capacity of the impeller but, given the specific geometry of the hyperboloid impeller, this is not so adequate as discussed by Pinho et al. (1997). The circulation flow rate is usually normalized into the circulating flow number Fl_c of Equation (4)

$$Fl_c = \frac{\dot{Q}_c}{ND^3} \tag{4}$$

The circulating flow number and the corresponding Newton number can be combined into efficiency numbers that allow the comparison of different types of impeller. Two such ratios (E_2 and E_c) were determined, given by expressions (5) and (6) taken from Jaworski et al. (1996).

$$E_2 = \frac{Fl_c^3}{Ne} \tag{5}$$

$$E_c = \frac{Fl_c^3}{Ne}\left(\frac{D}{T}\right)^4 \tag{6}$$

For Newtonian fluids, the mean flow in this stirred vessel is complex and three-dimensional, but can be typified into the following sum of basic flow patterns: superimposed on a general rotating flow in the centre of the vessel, created by the impeller rotation, there is a vertical ascending movement of fluid along the vessel walls and a downwards motion at the centre, in the vicinity of the impeller axis (Pinho et al. 1997). Between these two regions stands the centre of circulation where the flow is fairly weak. This general pattern is characteristic of flows generated by axial impellers in combination with baffles (Oldshue, 1983).

To quantify this vertical motion as a circulation flow rate Q_c, it is necessary to measure radial profiles of the axial (vertical) component of the velocity vector (u_z) and obtain the maximum axial flow rate. Since the flow is rotationally symmetric, this flow rate is given by the following integration

$$\dot{Q}_c = \max\ \dot{Q}^+ \ \text{ or } \ \max\ \dot{Q}^- \text{ with} \tag{7}$$

$$\dot{Q}^- = 2\pi \int_{r_{shaft}}^{r_{(u=0)}} r u_z(r)dr \text{ and } \dot{Q}^+ = 2\pi \int_{r_{(u=0)}}^{r_{wall}} r u_z(r)dr$$

Conservation of mass ensures that both the positive and negative quantities are identical, within experimental uncertainty.

Experimental Facility and Instrumentation

Stirred Vessel

Geometric details of the stirred vessel and the coordinate system are schematically represented in Figure 1 (a). The experimental facility is the same as described in Pinho et al. (1997, 2000) except for a new more sensitive torquemeter. The vessel consisted of a 292 mm diameter T stirred vessel in acrylic, which was mounted on a support standing directly on a 3-D milling table. The vessel allowed a maximum height H of liquid of 600 mm, but the present measurements refer to H/T = 1 and D/T = 1/3. The vessel was mounted inside a square trough filled with water that played a double role: it reduced the amount of refraction in the laser beams of the laser-Doppler anemometer and it was also part of a heating and cooling circuit necessary to maintain a constant temperature of 25°C within the vessel. Within the tank, four 25 mm wide and 4 mm thick baffles were mounted at 90° intervals to avoid solid-body rotation of the fluid. The baffles were attached to small triangular connectors that separated them by 6 mm from the vessel wall, to eliminate the dead zones normally found behind the baffles. The bottom of the tank was flat and had a bearing embedded in it to support the drive shaft, thus minimizing shaft wobbling.

Two different impellers of 100 mm diameter D were investigated: the hyperboloid, that constitutes the main focus of interest in this paper, and a standard Rushton impeller that was used for some comparison purposes. Geometric details of the hyperboloid agitator are presented in Pinho et al. (1997) and Höfken and Bischof (1993). The hyperboloid was mounted on a 12 mm shaft, which had a small 8 mm diameter recess where the hyperboloid was fixed. The impeller was positioned with an off-bottom clearance to vessel diameter ratio of C/T = 1.3/30. The six-bladed Rushton impeller is shown in Figure 1 (b) and was mounted at the standard configuration of 1/3 off-bottom clearance (C/T = 1/3).

Power Measuring System

A 600 W DC servomotor powered the impeller and was controlled by a variable power supply unit. A tachogenerator gave an electrical impulse proportional to the speed and controlled it together with an amplifier. The analog output, from 0 to 10 V, corresponded to a speed in the range 0 to 3 000 rpm. The speed could be kept constant with an uncertainty of around ±1 rpm but never exceeded 600 rpm, except for very short periods of time, to avoid damage to the baffles.

The torquemeter, model T34FN/1 from HBM, had a full range torque of 1Nm and was free from friction losses because it consisted of a physically separated rotor and stator. The rotor (T34r40/1), where the strain gauge bridge was attached, was fixed to the shaft and was totally separate from the stator (T34ST), which comunicated in frequency with the rotor. The output from the torquemeter fed an MGC amplifier from HBM, and its output, as well as that from the tachogenerator, was fed to a computer via an A/D converter. Purpose-built software gave all the results, namely, the rotational speed, the torque and the power.

The measured torque included the torque transmitted to the fluid and the torque loss absorbed by the bearings. The

torque loss was subtracted from the total torque to yield the net torque, after measurements were carried out with the fluid level just above the bottom bearing, but without touching the impeller. Analysis of the uncertainties of these systems was combined to produce global relative uncertainties of the Reynolds and Newton numbers of ±10% and ±5% at the lowest Reynolds numbers, respectively. These uncertainties decreased as the Reynolds number increased.

Laser-Doppler System

A 1-D Laser-Doppler anemometer was used to measure radial profiles of the axial velocity of some of the flows. The DANTEC LDA system was used in the forward scatter mode and the light source was an air-cooled, multimode 100 mW Ar-ion laser. The beam passed through a series of optical elements before the Bragg cell, where a frequency shift of 0.6 MHz was imposed. To improve the alignment of the optics and reduce the size of the control volume a pinhole section and beam expander, with an expansion factor of 1.95, were put before the 600 mm front lens.

The scattered light from titanium dioxide 3 μm mean diameter seeding particles was collected by the photo-multiplier before which stood an interference filter of 514.5 nm. For the non-Newtonian solutions it was not necessary to seed the flow with the TiO_2 particles. After being band-pass filtered the signal from the photo-multiplier was processed by a TSI 1990C counter operating in the single measurement per burst mode with a frequency validation setting of 1% in the 10/16 cycle comparison. A 1400 Dostek card interfaced the counter with a 80486 based computer to provide all the statistical quantities via a purpose-built software. The refraction of the laser beams in the plane walls of the trough and in the curved walls of the vessel was taken into account to correct the position of the control volume. Table 1 provides the main characteristics of the Laser-Doppler anemometer.

Table 1. Main characteristics of the Laser-Doppler anemometer in air at e^{-2} intensity

Laser wavelength	514.5 nm
Measured half angle of beams in air	3.65°
Dimensions of measuring volume in air	
– major axis	2.53 mm
– minor axis	162 μm
Fringe spacing	4.041 μm
Frequency shift	0.6 MHz

The LDA measurements were carried out at locations far from the impeller where, for Newtonian fluids, the flow was found to be angle-independent by Pinho et al (2000). Therefore, in this work all measurements of the mean and rms values of the instantaneous velocity were obtained with 360° ensemble-averaged measurements from a sample size of 28,000 valid readings. This large sample was necessary for accurate results, because of the low velocities and high levels of local turbulence encountered in the region. All velocity measurements were taken in the vertical mid-plane between two adjacent baffles.

Rheometer

The rheological characterization of the fluids was carried out in a Physica rheometer, model Rheolab UM/MC100. The double gap concentric cylinder system Z1-DIN was used for the dilute solutions andd the cone-plate system (MK-22) for the concentrated solutions. The double-gap cylinder measures shear stresses up to 67 Pa, but the lower end of the range is limited to a stress of the order of 1% of the full scale for reasons of accuracy. The maximum shear rate is 4,031 s^{-1}. The system was operated in controlled stress mode and a thermostatic bath maintained the temperature of the sample at 25°C and controlled its variation to within ±0.1°C.

Measurements of the viscometric viscosity (η) in steady shear flow and of the storage (G') and loss (G'') moduli in oscillatory shear flow were carried out. For some of the dilute solutions, measurements of η, G' and G'' were also carried out in the more accurate rheometer, model AR1000 from TA at the University of Liverpool (Escudier et al. 2001). The total uncertainty of the viscosity measurements taken in the Physica rheometer varied from 6% to less than 0.4% and from 9.4% to 1.42% as γ increased from 10 to 3300 s^{-1} for the 0.4% CMC and 0.25% XG solutions, respectively. For the TA instrument the uncertainty was below 2% (Escudier et al. 2001).

Fluids

Fluid Preparation

Measurements of the power consumption were carried out with various aqueous polymer solutions based on three different polymers, but only with two of them (0.2% CMC and 0.2% XG) the flow circulation and turbulence were investigated. To prevent bacteriological degradation, 0.02% by weight of the biocide Kathon LXE from Rohm and Haas was added to all fluids. The following fluids were investigated where the concentrations are by mass:

- 0.2%, 0.4% and 0.6% solutions of the low molecular weight (6,000 g/mole) methyl hydroxyl cellulose, brand name tylose, grade MH10000K, from Hoechst. Tylose is a small molecule with a glucose-based backbone, and more details can be found in Pereira and Pinho (1994);
- 0.2%, 0.3% and 0.4% solutions of moderate molecular weight (300,000 g/mole) carboxymethyl cellulose sodium salt, brand name CMC, grade 7H4C, from Hercules. CMC is a branched semi-rigid molecule, but is longer than the molecule of tylose. More details can be found in Escudier et al (2001) and Tam and Tiu (1989);
- 0.1%, 0.2% and 0.25% of the high molecular weight (2×10^6 g/mole) xanthan gum (XG), brand name Keltrol, grade TF from Kelco. Xanthan gum is a polysaccharide produced by the action of a bacteria and is also a semi-rigid, long molecule. More details on this polymer and its solutions can be found in Lapasin and Pricl (1995) and Escudier and Smith (1999);
- For the determination of the impeller parameter k concentrated solutions of xanthan gum (3.6%) and CMC (5.2%) were necessary in order to attain the laminar regime, as explained before.

All solutions were prepared with Porto tap water following the same procedure. The additives were added slowly to the water while being stirred, after which the mixture was agitated for a further 90 minutes. Then, the solutions rested

for 24 hours to ensure complete hydration of the molecules, and prior to any rheological or hydrodynamic measurement the solutions were agitated again for 30 minutes to fully homogenise them.

For comparative purposes three Newtonian fluids were used in experiments having the following properties at 20°C: pure water (ρ = 1000 kg/m^3, η = 0.00102 Pas), a mixture of glycerin and water (ρ = 1140 kg/m^3, η = 0.0117 Pas) and pure glycerin (ρ = 1200 kg/m^3, = 0.669 Pa·s). During the experiments the temperature was monitored in order to accurately determine the correct fluid poperties from the corresponding measurements at different temperatures.

Fluid Rheology

Measurements of the viscometric viscosity were carried out for all the dilute solutions of tylose, CMC and xanthan gum as a function of shear rate, the results of which are plotted in Figure 2 only for the most concentrated of the tested solutions.

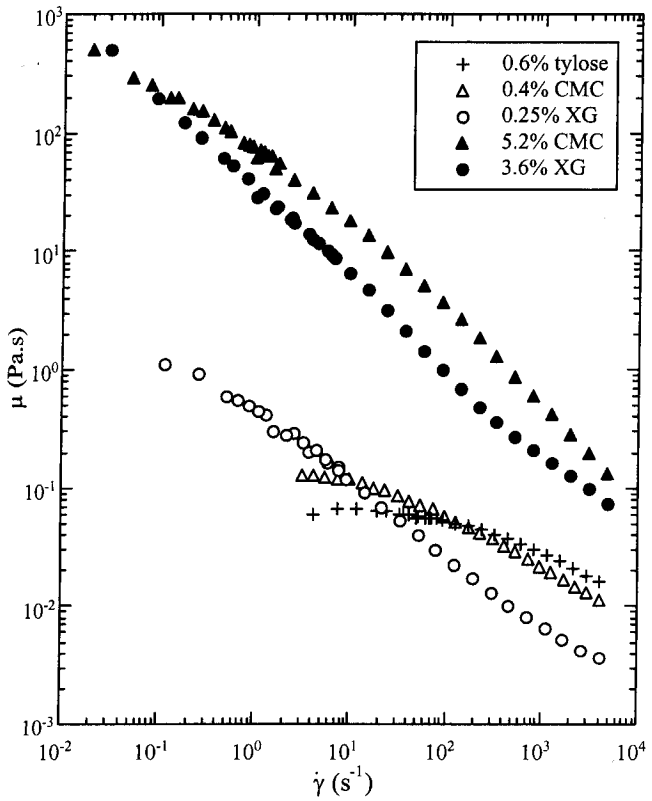

Figure 2. Measured viscometric viscosity of some polymer solutions at 25°C.

Viscosity models were fitted to the measured data by a least-squares method. For the tylose and CMC solutions the simplified Carreau model (Equation (8)) was used since the data showed the low shear rate plateau followed by the power law region. For the xanthan gum solutions the Sisko model of Equation (9) provided a better fitting. The parameters of the adjusted viscosity models are tabulated in Tables 2 and 3, respectively.

$$\eta = \mu_0\left[1+\left(\lambda_c\dot{\gamma}\right)^2\right]^{(n_c-1)/2} \tag{8}$$

$$\eta = \mu_r\left(\lambda_s\dot{\gamma}\right)^{n_s-1} + \mu_\infty \tag{9}$$

For each polymer additive shear-thinning increases with polymer concentration and the least shear-thinning fluids are those made from tylose, as expected due to their lower molecular weight, whereas the XG solutions exhibit the strongest shear-thinning intensity: notice that for XG the first Newtonian plateau is not yet observed in contrast to the CMC and tylose solutions. At high shear rates, however, these same xanthan gum solutions became the less viscous, or as viscous as the thin 0.2% tylose solution.

Table 2. Parameters of the adjusted simplified Carreau model

Fluid	μ_0 [Pa·s]	λ_c [s]	n_c	$\dot{\gamma}$ [s^{-1}]
0.2% CMC	0.02652	0.03053	0.697	15-4031
0.3% CMC	0.08533	0.23517	0.717	7-4031
0.4% CMC	0.14097	0.11376	0.618	3-4031
0.2% tyl	0.00463	0.00377	0.900	20-4031
0.4% tyl	0.01865	0.00713	0.783	15-4031
0.6% tyl	0.06268	0.01468	0.697	4-4031

Table 3. Parameters of the adjusted Sisko model.

Fluid	μ_r [Pa·s]	λ_s [s]	μ_∞* [Pa·s]	n_s	$\dot{\gamma}$ [s^{-1}]
0.1% XG	1.86	1970	0.001	0.543	3-2700
0.2% XG	31.47	2909	0.001	0.417	0.5-4031
0.25% XG	98.54	1700	0.001	0.326	0.1-4031

* Viscosity of solvent

Figure 2 also includes the viscosity data for the concentrated CMC and XG solutions. Shear-thinning is now stronger and, even for the CMC solution the low shear rate plateau was not observed within the measured range of shear rates.

The determination of the impeller constant of Metzner and Otto (1957) is facilitated by fitting the viscosity data of these viscous fluids by a power law having consistency index K and power index n. The corresponding parameters are listed in Table 4.

Table 4. Parameters of the power law adjusted to the concentrated XG and CMC solutions.

Fluid	K [Pa·s^n]	n
3.6% XG	34.0	0.25
5.2% CMC	71.3	0.30

Regarding fluid elasticity, measurements in oscillatory shear flow for the more concentrated of the dilute solutions are reported elsewhere: for the 0.6% tylose Coelho and Pinho (1998) found basically a viscous fluid with the ratio of the loss over the elastic moduli G'/G'' ~ 3 to 5 and a value of G' of 0.12 Pa at 10 Hz, but the accuracy of the rheometer used was rather poor and the measurements were limited to the range of 5 to 20 Hz. Benefitting from more recent instruments Escudier et al. (2001) confirmed and extended the results of Coelho and Pinho (1998). The 0.4% CMC solution was more elastic than the 0.6% tylose and, in the range 0.01 to 50 Hz G''/G' decreased from 11 to 1.25 on increasing the frequency: $G' \approx 0.0024$ Pa and $G'' \approx 0.027$ Pa at 0.1 Hz, and $G' \approx 3.2$ Pa and $G'' \approx 4.0$ Pa at 50 Hz, respectively.

The larger, more branched xanthan gum molecules yielded more elastic and viscous solutions in this near-rest rheological test: at 0.01 Hz, $G' \approx 0.02$ Pa and $G'' \approx 0.048$ Pa, but at a frequency of 50 Hz the elastic stress was higher than the viscous stress ($G' \approx 3.2$ Pa against $G'' \approx 1.8$ Pa).

Results and Discussion

Power Consumption

Newtonian Flow

In order to verify the values of the Newton number, power measurements were carried out first for Newtonian fluids using both the Rushton and the hyperboloid impellers, and the results are presented in Figure 3.

For the Rushton impeller the measured values agree with literature data and in particular with those reported by Hockey (1990) and Pinho et al. (1997) the latter using the same rig. However, note that the present measurements were obtained with a more accurate torquemeter than Pinho et al. (1997): the full scale of the torquemeter was 1 Nm, Pinho et al's instrument could measure up to 50 Nm with an accuracy of 10^{-2} Nm.

The hyperboloid is a low power agitator, with a consumption more than five times lower than that of the Rushton at high Reynolds numbers, and this has been confirmed again. In Figure 3 the present data are compared with Equation (7a) of Pinho et al. (1997), which was fitted to the extensive set of data for the hyperboloid. The present data are 10% below the correlation of Pinho et al. (1997) tending to $Ne = 0.8$, whereas the previous data became asymptotic to 0.88 at high Reynolds number. The higher accuracy and better experimental procedure of the present measurements lead us to conclude that the present data are to be preferred to those of Pinho et al. (1997) and, consequently the new data were fitted by an expression of the same type

$$Ne = 0.81 + \frac{86.6}{Re} + \frac{87.9}{Re^2} \qquad (10)$$

which is also represented in Figure 3 as a full line.

Non-Newtonian Rushton Impeller Flow

For the Rushton impeller, the value of k was determined by Metzner and Otto (1957), Calderbank and Moo-Young (1959) and Godleski and Smith (1962), and in 1961 Metzner et al. concluded that the choice of a value between 11.5 and 13 was not critical since a 30% variation in k resulted in a smaller variation in the viscosity of shear-thinning fluids (of 12% for $n = 0.5$). Here, a value of $k = 12$ will be used together with

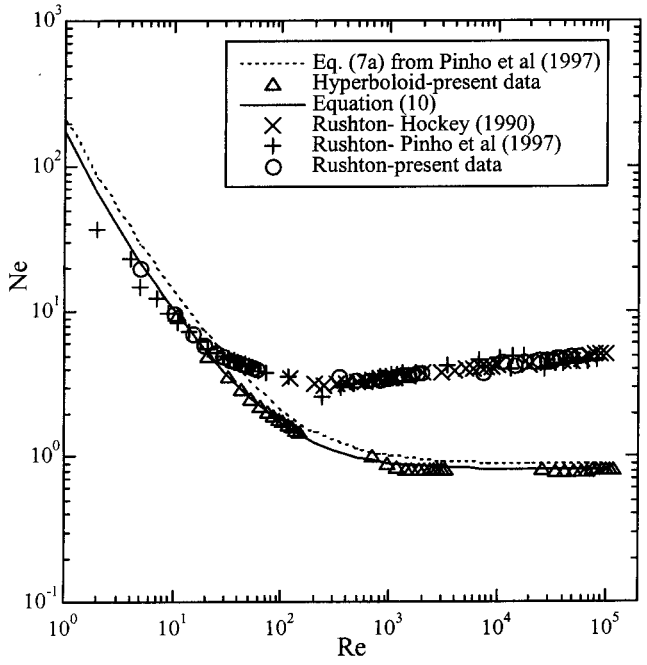

Figure 3. Newton number as a function of Reynolds number for Newtonian fluid flows with the Rushton and hyperboloid impellers with $H/T = 1$ and $D/T = 1/3$.

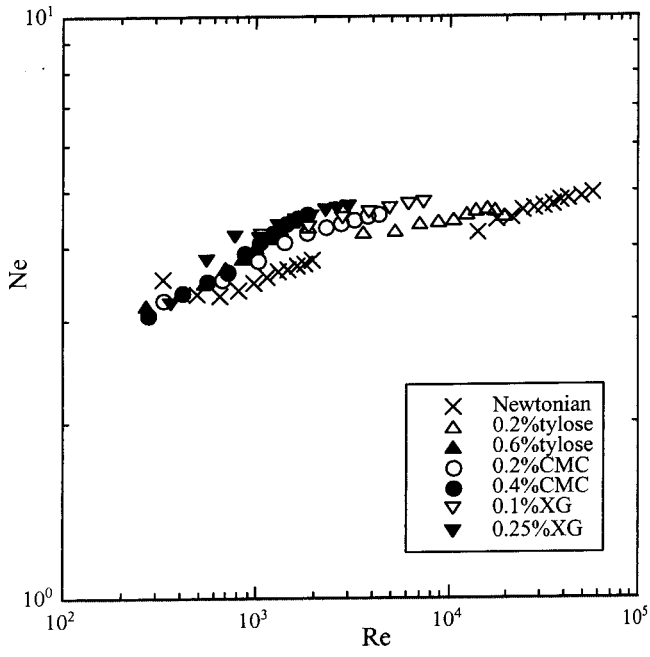

Figure 4. Variation of the Newton number with the Reynolds number in stirred vessels agitated by a Rushton impeller in the standard configuration ($H/T = 1$, $D/T = 1/3$) with some solutions.

Equation (3), the rheograms of the fluids and the definition of Reynolds number in Equation (1) to determine *Re*. Figure 4 compares the variations of the *Ne-Re* data for polymer solutions and two Newtonian fluids.

The figure shows that for all solutions there is an increase in Newton number relative to the Newtonian flow case, with XG exhibiting the largest differences, and that polymer concentration also raises the power consumption. At low Reynolds numbers the data for CMC and tylose crosses over that of Newtonian fluids. This intermediate Reynolds number range corresponds to transition from the laminar flow to the high Reynolds number turbulent flow: here Hockey (1990) also found, for a 0.4% CMC solution of the same brand, a complex transitional behaviour with his data approaching the Newtonian data at various places but in different ways. In his plot the CMC solutions also show a higher Newton number than the Newtonian fluids. The present measurements are more restricted than those of Hockey (1990), but are in agreement with the reported complex behaviour.

Characteristic Hyperboloid Parameter, k

For each power measurement with the concentrated CMC and XG solutions the Newton number was calculated and set identical to a Newtonian value from which a Reynolds number was obtained using a fit to the *Ne-Re* data for the viscous Newtonian fluid. With the same rotational speed the viscosity of the viscous Newtonian fluid was calculated and set equal to the apparent viscosity of the concentrated polymer solution. Next, using the rheogram for each fluid and Equation (3) the corresponding values of γ_c and k were determined. In Figure 5 a plot of the characteristic shear rate as a function of N shows for both fluids that at low rotational speeds the variations are linear and have similar slopes but at higher speeds the behaviour is non-linear and these data should not be used to determine the value of k. The straight line represents Equation (3) with $k = 27.2$, which is the average of the 5 lowest data for 3.6% XG ($k = 27.9$) and 5.2% CMC ($k = 26.4$). These values correspond to Reynolds numbers between 3 and 25 for the 5.2% CMC solution and 3 and 50 for the 3.6% XG solution. The average value of k represents the k data within 15%.

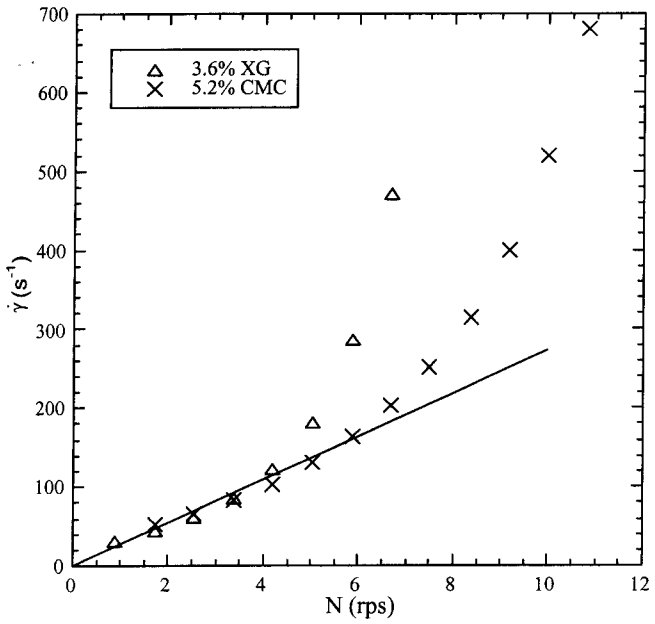

Figure 5. Variation of the characteristic shear rate with rotational speed for the two viscous polymer solutions and comparison with Equation (3).

The non-linear variation of the $\gamma_c - N$ plot at higher rotational speeds corresponds to higher Reynolds numbers where the flow becomes transitional, as can be assessed in Figure 3. The uncertainty in the value of k is similar to that found in the literature for other impellers, as documented in Rieger and Novák (1973) although slightly on the high side because for data on the same mixing system, the uncertainty in k is usually around 10% and this includes already the effect of shear-thinning (see also Metzner et al. 1961).

In order to improve the above value of k, further measurements must be carried out with more viscous solutions of these and other polymers together with a proper quantification of the first normal stress difference coefficient in order to separate Reynolds and Deborah number effects.

Non-Newtonian Hyperboloid Impeller Flow

Using the newly defined value ($k = 27.2$) the results of the power measurements can now be presented. Figure 6 plots the variation of the power number with the generalised Reynolds number of Otto and Metzner (1957) for the tylose, CMC and xanthan gum solutions, respectively. In each graph the solid line represents the Newtonian behaviour, Equation (10). The plots show a decrease in the Newton number of about 13%, especially for the CMC solutions, but the decrease is absent from the less elastic 0.2% tylose.

In general, at Reynolds numbers in the range 10^3 to 10^4 the power number for the polymer solutions attain values of the order of 0.7 and less, whereas for Newtonian fluids it is always higher than the asymptotic high Reynolds number value of 0.81. For the tylose solutions the power number increases with Reynolds number and approaches the Newtonian curve at the upper range. Note that these solutions are the less elastic and shear-thinning of all. For the CMC, however, although there is a slight tendency for *Ne* to increase with *Re*, the *Ne* asymptotes to a lower value below the Newtonian curve. Finally, for the xantham gum *Ne* starts at values lower than those of the Newtonian fluids at Reynolds numbers around 3,000, then it increases and at Reynolds numbers in excess of 20,000 the power number of the 0.1% XG is close but still below the Newtonian curve.

A feature common to all plots is that the less concentrated solutions have a tendency to higher power numbers at the low end of the Reynolds number range. One or two data points are above the Newtonian curve: these points were always measured at very low rotational speeds, where the experimental uncertainty and noise are the highest.

The power number reductions of the polymer solutions are not totally unexpected. These same solutions exhibit drag reductions in excess of 40% in fully developed turbulent pipe flow, Pinho and Whitelaw (1990), Pereira and Pinho (1994), Escudier et al. (1999). Whereas the flow in the pipe is completely dominated by wall-effects, here the wall has a far lesser impact on flow characteristics and power consumption. The wall that most matters is that of the impeller where the

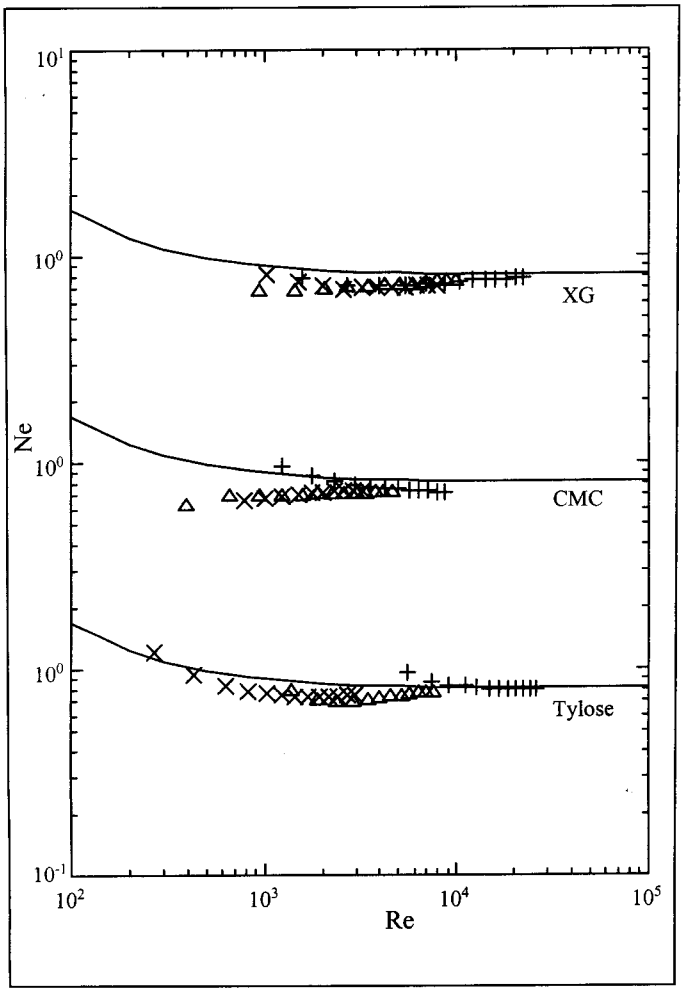

Figure 6. Variation of the Newton number with the Reynolds number in stirred vessels agitated by one hyperboloid impeller in the standard configuration (H/T = 1, D/T = 1/3): + 0.2% tylose, 0.2% CMC, 0.1% XG; Δ 0.4% tylose, 0.3% CMC, 0.2% XG; X 0.6% tylose, 0.4% CMC, 0.25% XG. Line represents Equation (10).

flow is attached, but the molecules only stay in this boundary-layer for very short periods of time. Nevertheless, it is still remarkable that about 10% of power reduction is observed with the more elastic solutions of CMC and XG.

With the Rushton turbine, on the other side, the shorter blades and more violent flow in the impeller region result in shorter residence times of the fluids in the attached boundary-layers and the flow is usually separated from the blades. Now, there is no power reduction, but a power increase which may result from transitional effects and a different flow pattern in the vicinity of the impeller.

In spite of its longer molecule, XG is semi-rigid whereas CMC molecules are flexible. This produces higher elasticity for XG than for CMC in near-rest flows, as during the measurements of G' and G" at low frequencies, but otherwise the flexibility of CMC molecules impart a higher elastic effect on the flow. This is consistent with the measurements of extensional viscosity and drag reduction in turbulent pipe flow of Escudier et al. (1999) using similar XG and CMC fluids.

The role of fluid elasticity under turbulent flow conditions is different from that found in laminar flow as a review of literature on pipe flow drag reduction shows (Gyr and Bewersdorff, 1995; Warholic et al. 1999; Ptasinski et al. 2001 amongst others). Whereas in laminar flow, the normal stress effects due to shear are related to the different flow features found, under turbulent flow conditions it is most probably the extensional viscosity that plays the main role. So far there has been no definite experimental proof of this theory, but the recent DNS simulations show that significant amounts of drag reduction require constitutive models having strain-thickening extensional viscosities, or at least Trouton-thickening viscosities (Dimitropoulos et al. 2001). A major problem in correlating these rheological and hydrodynamic properties is the measurement of true extensional viscosities for the dilute solutions required to attain turbulent flow. An indirect method, such as the measurement of $f - Re$ in turbulent pipe flow, remains a qualitative alternative to assess the relevance of elastic effects in turbulent flow as done here.

Flow Circulation

Since the hyperboloid mixer is close to the bottom of the vessel (C/T= 1.3/30, see Figure 1 (a), measurements of the axial velocity component were carried out at various horizontal planes above the impeller base plane, in the range z/R = 0.6 to 2.0. It was in this region that Pinho et al. (1997) found the highest axial flow rates for water, in particular near z/R = 1. Axial velocity measurements were carried out with water, to compare with Pinho et al. (1997), and more extensively with the solutions of 0.2% XG and 0.2% CMC, to analyze the polymer effect. All velocity data are normalised by the impeller tip speed U_{tip}.

A first impression of the differences between the Newtonian and non-Newtonian flow fields can be grasped in Figure 8 measured at z/R = + 1.4. The figure compares a Newtonian flow at 300 rpm and the 0.2% xanthan gum flow at 500 rpm, but the corresponding Reynolds numbers differ by a factor of 9. At speeds in excess of 650 rpm unnecessary strain was put into the perspex baffles and, for protection, these high speeds were only used during the short periods required for the power measurements, but not for velocity measurements. In the centre of the vessel the negative velocities pertain to the descending flow and are similar, with the flow of the xanthan gum slightly slower than the water flow. In the wall jet, the peak velocity of the ascending flow is higher (faster) for the water and occurs closer to the wall than for the polymer solution. However, the main significant difference is in the turbulent flow field: across the whole vessel the normalized axial turbulence for the xanthan gum solution is less than half that of the water flow. The turbulence of the xanthan gum is so low that its rms profile becomes very sensitive to mean gradient broadening effects near the vessel wall as will be shown later. The Newtonian profiles were compared with the data from Pinho et al. (1997) and the differences were negligible and within the experimental uncertainty. Although the Reynolds numbers are different, they both pertain to the inertia-dominated regime and for a Newtonian fluid it is turbulent at a Reynolds number of 5,950, identical to that of 0.2% XG (Pinho et al. 1997, 2000). Besides, as often happens with Newtonian turbulent flows, the turbulence at Re = 5 950 is most likely higher than that at 52 400, which reinforces our argument.

From these and similar profiles at other z- planes the axial flow rate was calculated in both the ascending (wall jet) and descending flow regions (centre of the vessel) and the

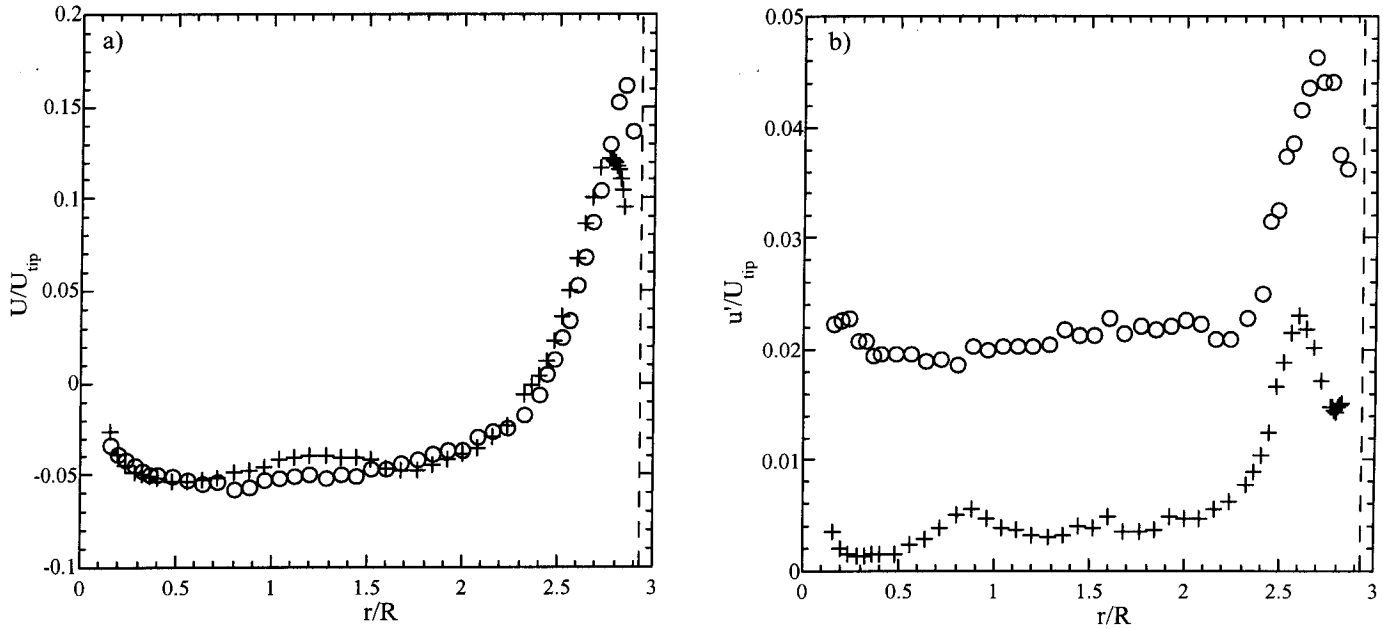

Figure 7. Radial profiles of the mean (a) and rms (b) axial velocity component at $z/R = +1.4$ for: water, $Re = 52\,400$ (O); 0.2% XG, $Re = 5\,950$ (+). Vertical dashed line marks vessel wall location.

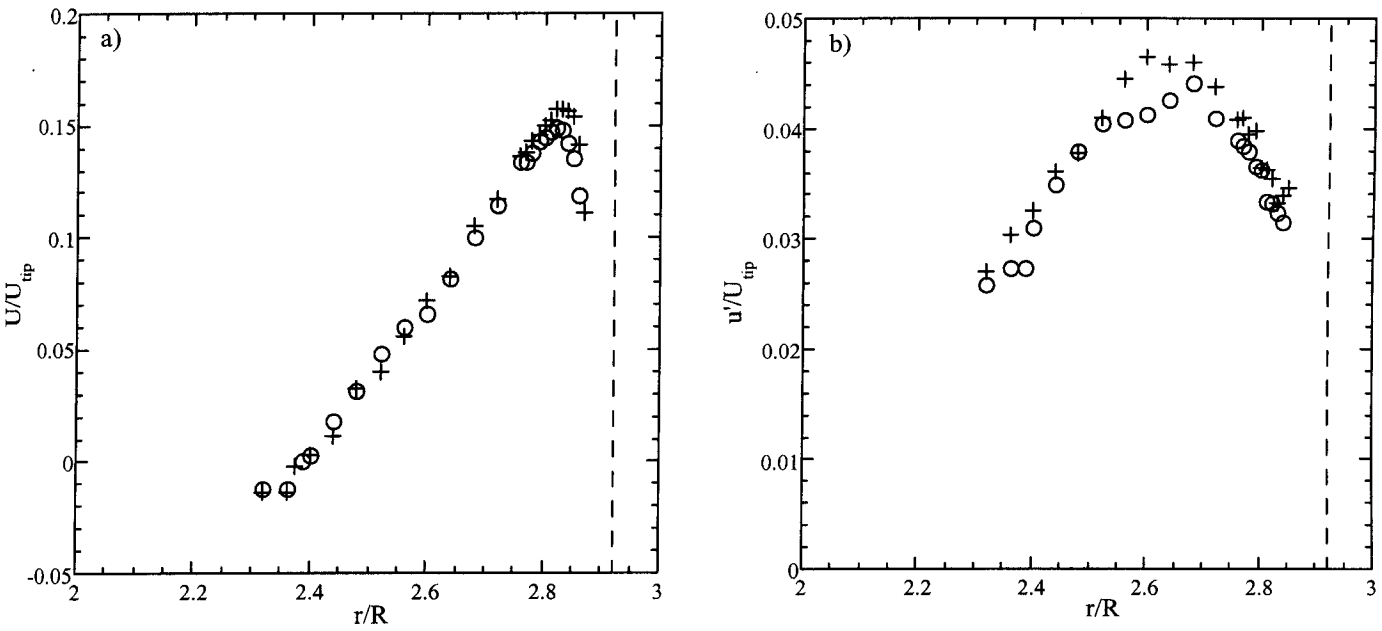

Figure 8. Radial profiles of the mean (a) and rms (b) axial velocity component at the wall jet for water flow at $z/R = +1$: $Re = 56\,200$ (O); $Re = 93600$ (+). Dashed line marks vessel wall location.

differences were found to be less than 10%. Since it was not possible to measure very close to the impeller in forward scatter, and to obtain valid LDA signals in backscatter for the less clear polymer solutions, it was decided to perform the remaining measurements of axial velocity, aimed at determining the circulating flow rate, only in the wall jet region. This required careful measurements in the wall region because of its large contribution to the flow rate.

The Newtonian flow at the wall jet is compared at two diferent high Reynolds numbers in Figure 8. In both cases the turbulent flow is well developed and, consequently, the dependence of the normalized mean and rms velocities is very weak and only detected in the slightly higher peak values at the highest Reynolds number. In this and in subsequent figures, the velocity data are plotted only in this wall jet region.

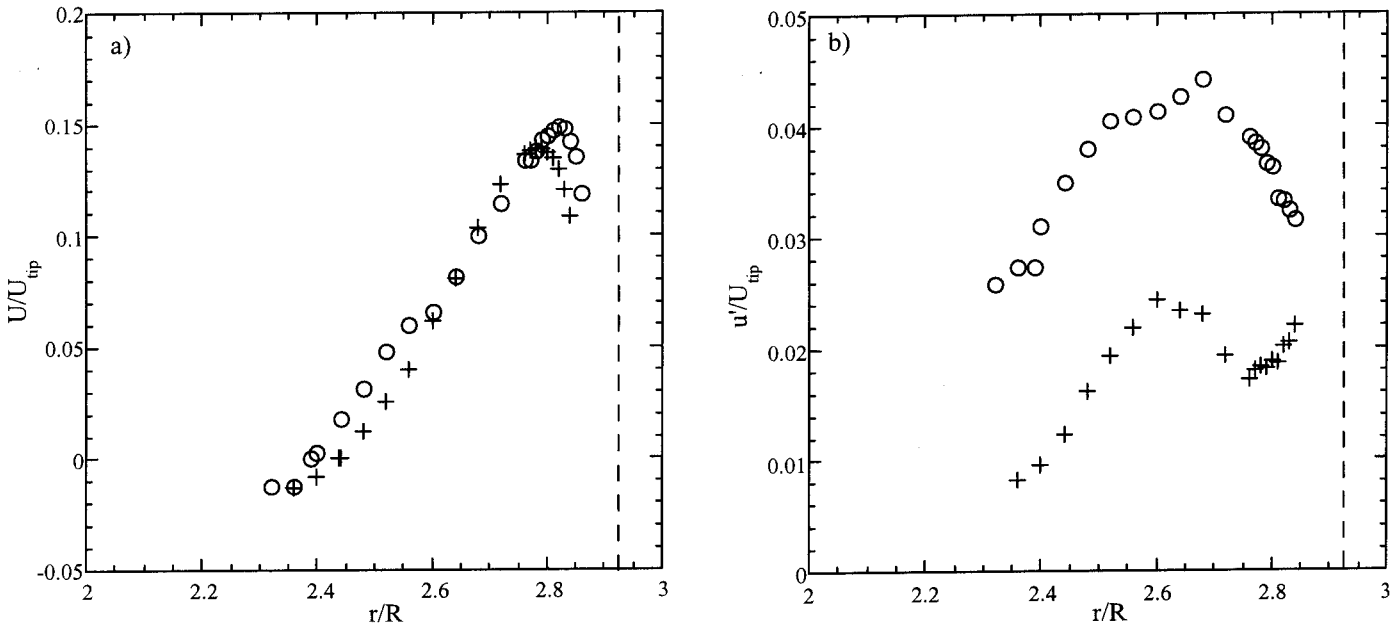

Figure 9. Radial profiles of the mean (a) and rms (b) axial velocity component at the wall jet and z/R = + 1.0 for: water, Re = 52 400 (O); 0.2% XG, Re = 5,950 (+). Vertical dashed line marks vessel wall location.

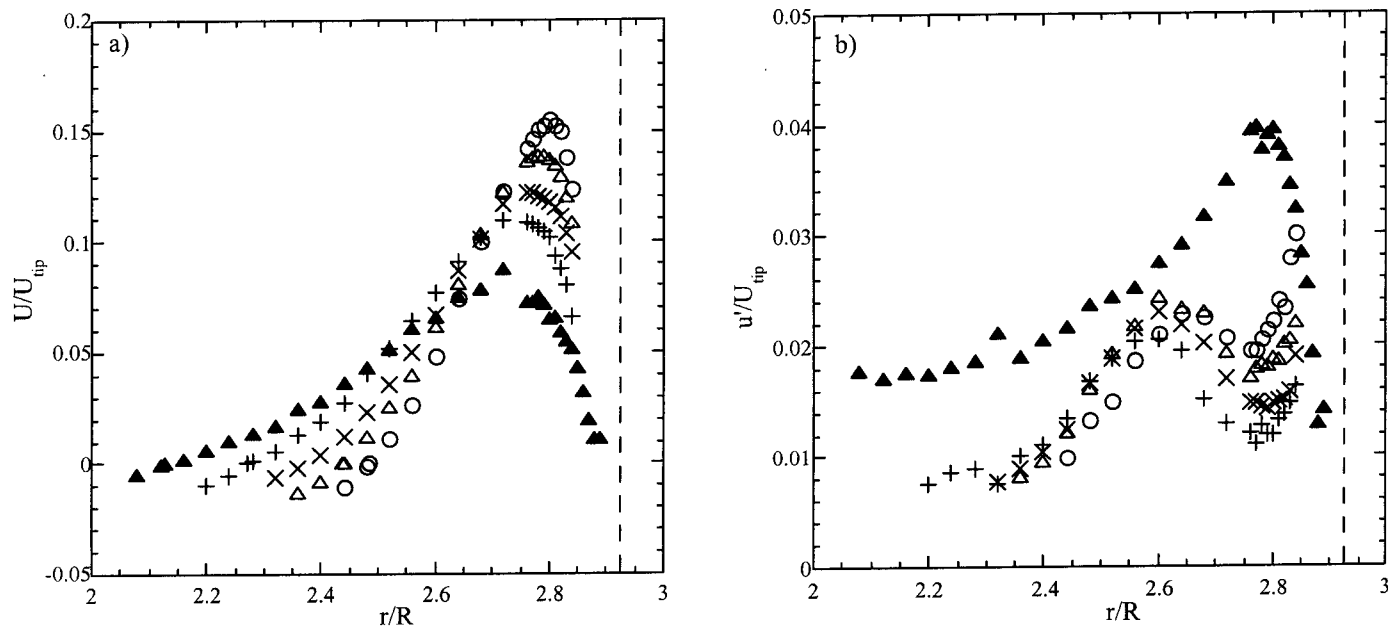

Figure 10. Effect of height and polymer additive on the radial profiles of the mean (a) and rms (b) axial velocity component at the wall jet for 0.2% XG at Re = 5 950: z/R = 0.6 (O); z/R = 1 (Δ); z/R = 1.4 (X); z/R = 1.8 (+); 0.2% CMC and Re = 4 560 at z/R = 1 (solid Δ). Vertical dashed line marks vessel wall location.

Figure 9 corresponds to the flow conditions of Figure 7 but at a different height (z/R = 1) and shows only the wall jet. The picture described in Figure 7 emerges again: the mean flows are not very different but the turbulence is basically half of that found with water and the above-mentioned mean gradient broadening effect is now more clear (rise in rms near the wall), an indication that the true turbulence is smaller. Note also that the peak turbulence for the XG solution occurs farther away from the wall than for the water, which is also consistent with the different Reynolds numbers.

The development of the wall jet with height is represented in Figure 10 (a), which plots the radial variation of the normalized axial mean velocity for increasing values of z/R. As z/R increases from 0.6 to 1.8 the peak velocity near the wall

decreases by a factor of a third, from 0.16 to 0.11, and the normalized width δ/R of the jet increases from 0.44 to 0.65. The corresponding rms profiles show a decreasing turbulence with z/R, especially very close to the wall, which is due to a decrease in mean gradient broadening because on moving upwards the velocity profiles are less steep. Nevertheless, these differences occur because of the low turbulence intensity of the 0.2% XG solution flow as it reaches the wall jet. Whether this low turbulence is due to a lower turbulence production in the impeller region or a faster dissipation subsequently, or both, requires a more extensive investigation. This effect of mean gradient broadening on the turbulence rms data is analyzed below.

Figure 10 includes one profile for a 0.2% CMC solution at $z/R = 1$ and at a lower but not too different Reynolds number of 4,560. It should be compared with the corresponding profile for the xanthan gum at z/R=1. The CMC profile is typical of a more turbulent flow, i.e. the jet is wider and less peaky, but the real difference is in the normalized rms profile that is well above all the profiles for the xanthan gum solution. The peak normalized rms for the CMC is 0.04, which is only 10% lower than that seen in Figure 9 for the water flow at $Re = 52\,400$. Given the small dependence of turbulence for Newtonian fluids on the Reynolds number there is clearly a small difference between CMC and Newtonian behaviour and a large difference between XG on one end and CMC and Newtonian fluids on the other. Since the mean velocity profile is also less steep for the CMC than for the xanthan gum the gradient broadening effect is less severe and this shows well especially near the wall where the tendency for a rise in rms only appears very close to it.

To assess the effect of mean gradient broadening, the rms data of Figure 10 was corrected, according to Durst et al. (1981), using Equation (11)

$$\sigma_m^2 = \sigma_t^2 + \sigma_g^2 + \sigma_o^2 \tag{11}$$

where σ_m^2 and σ_t^2 represent the measured and the true velocity variance, with the broadening effect σ_g^2 given by

$$\sigma_g^2 = \left(\frac{l_m}{4}\right)^2 \left(\frac{du_z}{dr}\right)^2 + \ldots \tag{12}$$

with l_m representing the length of the LDA control volume. Other effects to the broadening of variance (σ_o^2) were not considered.

All the rms data in Figure 10 (b) are replotted in Figure 11 after application of the mean gradient broadening effect correction and the results confirm our reasoning. For the xanthan gum solutions the data have dropped dramatically, except for a few data points near the wall. The missing data, in comparison with Figure 10 (b), correspond to a zero rms or to data where the amount of correction was larger than the measured rms. In the calculation of the broadening effect the length of the LDA control volume in air was used, which is smaller than the length within the liquid due to refraction. For the CMC profile, however, since the rms plot in Figure 10 (b) does indeed correspond to true turbulence, the corrected rms profile has decreased only slightly.

At this stage one can only speculate about this dramatic difference but one certainly must take into account two

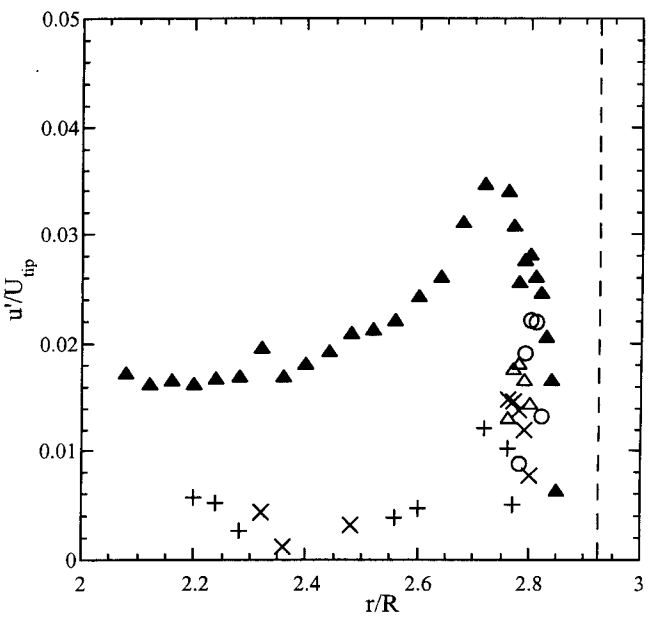

Figure 11. Radial profiles of normalized rms of Figure 10 (b) corrected for gradient broadening. Caption as in Figure 10.

possibilities: first, a power reduction was seen in Figure 6 that was attributed to the role of elasticity in turbulent flow, much in the same way as in the turbulent pipe flow of these fluids. There, under conditions of drag reduction there is also a decrease in the rms velocities but especially so for the radial and azimuthal components and not so much for the axial turbulence. It must be remembered that the semi-rigid structure of the XG offsets some of the impact of the large molecular weight of the XG solution on its high frequency elasticity and that under the high frequencies and shear rates encountered in turbulent flow it could even be less elastic than the CMC solutions. Anyway, both fluids reach similar amounts of drag reduction in turbulent pipe flow but in this case the wall presence is always felt.

In the vessel flow, the same drag reduction mechanism must certainly be acting to reduce turbulence below the Newtonian value along the boundary-layers, but the very strong and unexpected damping of longitudinal turbulence for the xanthan gum, and in comparison with the behaviour of the equally drag reducing 0.2% CMC solution, suggests a second mechanism. This is possibly explained by the very different low shear rate viscosity behaviour of the two fluids: whereas the 0.2% CMC tends to a Newtonian plateau of about 0.03 Pas (0.0265 Pas according to the data fitting), the low shear rate viscosity of the 0.2% xanthan gum solution is, by contrast, very high, with a value of 0.3 Pas at $\dot{\gamma} = 1\ s^{-1}$. It is known from the Newtonian results of Pinho et al. (1997, 2000) that at the inner edges of the bottom and wall jets, bordering the centre of the large recirculation in the vessel, the flow is rather weak. By their nature, shear-thinning fluids will accentuate this pattern and especially so the xanthan gum solutions which have a very intense shear-thinning and a very high Newtonian plateau. In these low velocity regions the turbulence dissipation is bound to be very intense, with the turbulence possibly decaying faster for the xanthan gum solution than for the CMC solution.

Efficiency

The mean flow data presented in Figures 8 to 10 allowed the calculation of the axial flow rate $\dot{Q}^+$ at various planes in the ascending flow region (positive velocities), the maximum of which is $\dot{Q}_c$ and is used to define the circulating flow number according to the formulae given initially. Whereas for the water flow Fl_c = 0.51 to 0.54 for Re = 50 000 to 90 000, consistent with the value of 0.57 obtained by Pinho et al. (1997) and within the experimental uncertainty, there was a decrease of about 20% for both the 0.2% CMC and 0.2% XG polymer solutions that showed values of Fl_c = 0.42 and 0.45, respectively. The energy input to the vessel is used for various purposes, such as generating the mean and the turbulent flows. Since the 0.2% XG flow is far less turbulent than the flow of 0.2% CMC it is not surprising that the mean flow of the former is stronger than that of the latter, as was seen in the wall jet profiles in Figure 10.

Since the decrease in Fl_c, due to the addition of polymer, was higher than the corresponding decrease in Ne, the two efficiency ratios were reduced in relation to that for Newtonian fluids. For the water flows E_2 = 0.2 and E_c = 0.0025 matching the values of Pinho et al. (1997), whereas for the CMC and xanthan gum flows E_2 varied from 0.1 to 0.12 and E_c from 0.0013 to 0.0014.

This important reduction in efficiency, of the order of 50%, together with the reduced turbulence in the wall jet for the xanthan gum solution and its implications regarding mixing quality, raises questions to the effectiveness of the hyperboloid as a mixer in waste water treatment plants. As has been demonstrated by Monteiro and Valente (1996), sludges found in waste water treatment plants usually have a yield stress. Although yield stress fluids were not used in the present investigation, the solutions of xanthan gum have a wide range of low shear rates where the fluid is still strongly shear-thinning. Thus, from an engineering point of view, in this flow the XG solutions approached well the expected behaviour of yield stress fluids.

Conclusions

Measurements of the power consumption, and of the mean and turbulent axial velocities, were carried out in stirred vessels powered by an hyperboloid impeller and operating with aqueous solutions of tylose, CMC and xanthan gum at concentrations ranging from 0.1% to 0.6% by weight. Some measurements were also carried out with a Rushton impeller as a check and for comparison purposes. The tylose solutions were the less elastic and shear-thinning with a wide first Newtonian plateau, whereas the xanthan gum solutions were so strongly shear-thinning that at shear rates lower than $1s^{-1}$ the viscosity was still increasing significantly. The following are the main conclusions of this work:

- The characteristic parameter k of Metzner and Otto (1957) for the hyperboloid impeller was determined and found to be equal to 27.2 ±15%;
- The Reynolds numbers of the polymer solution flows were rather low, between 1 000 and 10 000, and the flows were most likely transitional;
- With the Rushton turbine there was an increase in power consumption especially for the more elastic fluids based on CMC and XG, whereas for the tylose solutions the Newton number was barely unchanged from that of Newtonian fluids. For Reynolds numbers of about 1 000 to 4 000 the increase in Newton number varied between 13 and 20% ;
- With the hyperboloid impeller the opposite effect was observed. The power consumption decreased in comparison with the Newtonian behaviour, at identical Reynolds numbers in the range 10^3 to 3×10^4. This effect was more pronounced with CMC (flexible molecules), less so with xanthan gum (semi-rigid molecules) and even less with tylose (small flexible molecules). For each polymer, this power reduction was stronger with the more concentrated solutions, but never exceeded 13%. Given the shape of the hyperboloid impeller, its known Newtonian flow features and the characteristics of these same polymer solutions in turbulent pipe flow, we speculated that this reduction in power consumption is rooted on a reduction of friction drag over the hyperboloid surface, having similarities to the drag reduction phenomena of these same fluids in turbulent pipe flow. At higher Reynolds number flows, as form drag takes over, drag reduction effects tend to decrease;
- The measurements of the mean flow axial velocities for the 0.2% xanthan gum and CMC solutions showed a reduction of 25% in the circulating flow number, with the xanthan gum less affected;
- The efficiency numbers for the polymer flows, which combine the power consumption and the corresponding circulating flow rate, were reduced by a factor of 50% in relation to that of Newtonian fluids;
- Regarding the corresponding profiles of the rms of the axial velocity, whereas the turbulence of the xanthan gum solution was less than half of the turbulence of the water flow, both in the wall jet and in the centre of the vessel, the rms for the CMC solution was merely 10% lower than for the Newtonian flows in the wall jet. It was speculated that this dramatic difference between the behaviours of the CMC and XG solutions was mainly attributed to their different low shear rate viscosity. In fact, although at high shear rates the 0.2% xanthan gum solution is less viscous than the 0.2% CMC solution, at the low shear rates prevailing over the vast slow flow region of the vessel the local viscosities of the XG solution are at least ten times larger than those of the CMC solution.

Acknowledgements

The authors would like to thank the following financial support : JNICT – Junta Nacional de Investigação Científica – through project PEAM/C/TAI/265/93; and the scientific committee of the Mechanical Engineering Master Course of the Faculdade de Engenharia da Universidade do Porto. A.S. Cavadas has also benefitted from a research scholarship from JNICT.

Nomenclature

C	impeller off-bottom clearance, (m)
D	impeller diameter, (m)
De	deborah number
E_2	efficiency number
Ec	efficiency number
Fl_c	circulating flow number
Fr	Froude number
g	acceleration of gravity, (m/s^2)
G'	storage modulus, (Pa)
G''	loss modulus, (Pa)
H	height of liquid in vessel, (m)
k	Metzner and Otto's parameter

K	consistency index of viscosity power law, (Pa·s^n)
n	power exponent of viscosity power law
n_c	power exponent of simplified Carreau viscosity model
n_s	power exponent of Sisko viscosity model
N	rotational speed, (rps)
Ne	Newton or Power number
P	mixing power, (W)
Q_c	circulating flow rate, (m^3/s)
r	radial coordinate, (m)
R	radius of impeller, (m)
Re	Reynolds number
T	vessel diameter, (m)
u_z	z component of velocity, (m/s)
U_{tip}	impeller azimuthal tip speed, (m/s)
U	axial velocity component, (m/s)
z	vertical coordinate, (m)

Greek Symbols

λ	relaxation time of fluid
λ_c	time parameter of the simplified Carreau viscosity model, (s)
λ_s	time parameter of the Sisko viscosity model, (s)
$\dot{\gamma}_c$	characteristic shear rate in the impeller region, (s^{-1})
μ_0	zero shear rate viscosity in the simplified Carreau viscosity model, (Pa·s)
μ_r	second viscosity parameter in the Sisko viscosity model
μ_∞	infinite shear rate viscosity in the Sisko viscosity model, (Pa·s)
η	viscosity, (Pa·s)
η_c	characteristic or apparent viscosity, (Pa·s)
ρ	fluid density, (kg/m^3)
σ_g	broadening effect on velocity standard deviation, (m/s)
σ_m	measured velocity standard deviation, (m/s)
σ_t	true velocity standard deviation, (m/s)

References

Bertrand, F., P.A. Tanguy, E. Brito de la Fuente and P. Carreau, "Numerical Modeling of the Mixing Flow of Second-order Fluids with Helical Ribbon Impellers", Comput. Methods Appl. Mech. Engrg. **180**, 267–280 (1999).

Boger, D. V. and K. Walters, "Rheological Phenomena in Focus", Elsevier, Amsterdam, The Netherlands (1993)

Carreau, P. J., R. P. Chhabra and J. Cheng, "Effect of Rheological Properties on Power Consumption with Helical Ribbon Impellers", AIChE J. **39**, 1421–1430 (1993).

Calderbank, P.H. and M. B. Moo-Young, "The Prediction of Power Consumption in the Agitation of Non-Newtonian Fluids", Trans. Inst. Chem. Engr. **37**, 26–33 (1959).

Coelho, P.M. and F. T. Pinho, "Rheological Behaviour of Some Dilute Aqueous Polymer Solutions (in Portuguese)", Mecânica Experimental **3**, 51–60 (1998).

Dimitropoulos, C. D., R. Sureshkumar, A. N. Beris and R. A. Handler, "Budgets of Reynolds Stress, Kinetic energy and Streamwise Enstrophy in Viscoelastic Turbulent Channel Flow", Physics of Fluids **13**, 1016–1027 (2001).

Durst, F., A. Melling and J. H. Whitelaw "Principles and Practice of Laser-Doppler Anemometry", 2nd edition, Pergamon Press, New York, NY (1981)

Escudier, M.P., I. W. Gouldson, A. S. Pereira, F. T. Pinho and R. J. Poole, "On the Reproducibility of the Rheology of Shear-Thinning Liquids", J. Non-Newt. Fluid Mech. **97**, 99–124 (2001).

Escudier, M.P., F. Presti and S. Smith, "Drag Reduction in the Turbulent Pipe Flow of Polymers", J. Non-Newt. Fluid Mech. **81**, 197–213 (1999)

Escudier, M.P. and S. Smith, "Turbulent Flow of Newtonian and Shear-Thinning Liquids Through a Sudden Axisymmetric Expansion", Exp. in Fluids **27**, 427–434 (1999)

Godleski, E. S. and J. C. Smith, "Power Requirements and Blend Times in the Agitation of Pseudoplastic Fluids", AIChE J. **8**, 617–620 (1962).

Gyr, A. and H.-W. Bewersdorff, "Drag Reduction of Turbulent Flows by Additives", Series: Fluid Mechanics and its applications, Kluwer Academic Press, Dordreckt, The Netherlands (1995)

Hockey, R. M., "Turbulent Newtonian and Non-Newtonian Flows in a Stirred Reactor", PhD Thesis, University of London, U.K. (1990).

Höfken, M., F. Bischof, and F. Durst, "Novel Hyperboloid Stirring and Aeration System for Biological and Chemical Reactors", ASME – FED – Industrial Applications of Fluid Mechanics **132**, 47–56 (1991).

Höfken, M. and F. Bischof, "Hyperboloid Stirring and Aeration System: Operating Principles, Application, Technical Description", Invent GmbH report, version 1.1, Erlangen, Germany (1993).

Höfken, M., K. Zähringer and F. Bischof, "Stirring and Aeration System for the Upgrading of Small Waste Water Treatment Plants", Water Science and Technology **29**, 149–156 (1994).

INVENT Umwelt und Verfahrenstechnik GmbH& Co, http://www.invent-uv.de/

Ismailov, M., M. Schäfer, F. Durst and M. Kuroda, "Turbulent Flow Pattern of Hyperboloid Stirring Reactors", J. Chem. Eng. Japan **30**, 1090–1097 (1997).

Jaworski, Z., A. Nienow and K. N. Dyster, "An LDA Study of the Turbulent Flow Field in a Baffled Vessel Agitated by an Axial, Down-Pumping Hydrofoil Impeller", Can. J. Chem. Eng. **74**, 3–15 (1996).

Lapasin, R. and S. Pricl, "Rheology of Industrial Polysaccharides: Theory and Applications", Blackie Academic and Professional, U.K. London (1995).

Metzner, A.B. and R.E. Otto, "Agitation of Non-Newtonian Fluids", AIChE J. **3**, 3–10 (1957).

Metzner, A. B., R. H. Feehs, H. L. Ramos, R. E. Otto and J. D. Tuthill, "Agitation of Viscous Newtonian and Non-Newtonian Fluids", AIChE J. **7**, 3–9 (1961).

Monteiro, P. and J. T. Valente, "Flow Characteristics of Anaerobic Digesting Sludges", Proceedings of the 18th International Conference on Slurry Handling and Pipeline Transport – Hydrotranssport 18 – edited by J.F. Richardson, South Africa, 3–5 September, BHR Group Conference Series, 3–20 (1996).

Nouri, J.M. and J. H. Whitelaw, "Flow Characteristics of Hyperboloid Stirrers". Can. J. Chem. Eng. **72**, 782–791 (1994).

Oldshue, J.Y. "Fluid Mixing Technology", McGraw-Hill Book Company, New York, NY (1983).

Pereira, A.S. and F. T. Pinho, "Turbulent pipe flow characteristics of low molecular weight polymer solutions". J. Non-Newt. Fluid Mech. **55**, 321–344 (1994).

Pinho, F.T., F. M. Piqueiro, M. F. Proença and A. M. Santos, "Power and Mean Flow Characteristics in Mixing Vessels Agitated by Hyperboloid Stirrers", Can. J. Chem. Eng. **75**, 832–842 (1997).

Pinho, F.T., F. M. Piqueiro, M. F. Proença and A. M. Santos, "Turbulent Flow in Stirred Vessels Agitated by a Single, Low-Clearance Hyperboloid Impeller", Chem. Eng. Sci. **55**, 3287–3303 (2000).

Pinho, F. T. and J. W. Whitelaw, "Flow of Non-Newtonian Fluids in a Pipe", J. Non-Newt. Fluid Mech. **34**, 129–144 (1990).

Ptasinski, P. K., F. T. M. Nieuwstadt, B. H. A. A. Van Den Brule and M. A. Hulsen, "Experiments with Turbulent Pipe Flow with Polymer Additives at Maximum Drag Reduction", Flow, Turbulence and Combustion **66**, 159–182 (2001).

Rieger, F. and V. Novák, "Power Consumption of Agitators in Highly Viscous Non-Newtonian Liquids", Trans. Instn. Chem. Eng. **51**, 105–111 (1973).

Solomon, J., A. W. Nienow and G. W. Pace, "Flow Patterns in Agitated Plastic and Pseudoplastic Viscoelastic Fluids", I. Chem. E. Symp. Series **64**, A1–A13 (1981).

Tam, K.C. and C. Tiu, "Steady and Dynamic Shear Properties of Aqueous Polymer Solutions", J. Rheology **33** (2), 257–280 (1989).

Ulbrecht, J. J. and P. J. Carreau, "Mixing of Viscous Non-Newtonian Liquids", Chapter 4 in Mixing of Liquids by Mechanical Agitation, edited by J. J. Ulbrecht and G. K. Patterson, Gordon and Breach, New York, NY (1985).

Warholic, M. D., H. Massah and T. J. Hanratty, "Influence of Drag Reducing Polymers on Turbulence: Effects of Reynolds Number, Concentration and Mixing", Exp. in Fluids **27**, 461–472 (1999).

Zhou, G., P. A. Tanguy and C. Dubois, "Power Consumption in a Double Planetary Mixer with Non-Newtonian and Viscoelastic Materials", Trans. IChemE. **78**, Part A, 445–453 (2000).

Manuscript received June 27, 2002; revised manuscript received June 26, 2003; accepted for publication August 5, 2003.